AGU PUBLICATIONS

JGR

Journal of Geophysical Research: Atmospheres

RESEARCH ARTICLE
10.1002/2016JD024997

Key Points:
- Water transfer project reduces the falling rate of groundwater table
- Water transfer project slightly enhances the wetting and cooling effects
- The climatic changes are positively related to the transfer volume

Correspondence to:
C. Zhan,
zhancs@igsnrr.ac.cn

Citation:
Zou, J., C. Zhan, Z. Xie, P. Qin, and S. Jiang (2016), Climatic impacts of the Middle Route of the South-to-North Water Transfer Project over the Haihe River basin in North China simulated by a regional climate model, *J. Geophys. Res. Atmos.*, *121*, 8983–8999, doi:10.1002/2016JD024997.

Received 25 FEB 2016
Accepted 23 JUL 2016
Accepted article online 29 JUL 2016
Published online 12 AUG 2016

Climatic impacts of the Middle Route of the South-to-North Water Transfer Project over the Haihe River basin in North China simulated by a regional climate model

Jing Zou[1], Chesheng Zhan[2], Zhenghui Xie[3], Peihua Qin[3], and Shanshan Jiang[4]

[1]Institute of Oceanographic Instrumentation, Shandong Academy of Sciences, Qingdao, China, [2]Key Laboratory of Water Cycle and Related Land Surface Process, Institute of Geographic Sciences and Natural Resources Research, Chinese Academy of Sciences, Beijing, China, [3]State Key Laboratory of Numerical Modeling for Atmospheric Sciences and Geophysical Fluid Dynamics, Institute of Atmospheric Physics, Chinese Academy of Sciences, Beijing, China, [4]China Water Resources BeiFang Investigation, Design and Research Company Limited, Tianjin, China

Abstract The Middle Route of the South-to-North Water Transfer Project (MSWTP) was constructed to ease the water crisis over the North China Plain. In this study, we incorporated a water transfer scheme into the regional climate model RegCM4 and investigated the climatic impacts of the MSWTP over the Haihe River Basin in North China. Four 10 year simulation tests were conducted from 2001 to 2010 where different volumes of water were transferred. The results demonstrated that before the MSWTP was conducted the original groundwater exploitation and consumption over the Haihe River Basin led to wetting and cooling at the land surface with rapidly falling groundwater depth. The extra water input from the MSWTP slightly enhanced the wetting and cooling effects over the basin, as well as reduced the falling rate in the groundwater depth along the conveyance line. However, the weak climatic effects of the MSWTP were limited at a local scale and had no obvious interannual trends, because the transfer volume of the MSWTP was far lower than the total demand which has been conventionally satisfied through local water exploitation. In terms of seasonal variations, the greatest changes due to the MSWTP occurred in the summer for precipitation and soil moisture and in the spring for energy-related variables (heat fluxes and 2 m air temperature).

1. Introduction

The Middle Route of the South-to-North Water Transfer Project (MSWTP), which was launched at the end of 2014, was designed to transfer water northward from the Danjiangkou reservoir on the Han River in order to relieve the local water shortage crisis in North China [*Liu*, 1994]. The transferred water flows across Henan and Hebei Province, ultimately reaching Beijing and Tianjin, where the main conveyance canal has a length of 1277 km [*Wang et al*., 2006; *Shan et al*., 2007]. The intake area of the MSWTP covers about 1.55×10^5 km^2, and most of the intake area is located in the Haihe River basin. According to the Beijing Construction Committee Office of the South-to-North Water Transfer Project (http://www.bjnsbd.gov.cn/), the volume of water transferred is 9.5×10^9 m^3/yr in the current first stage of construction, and it will be 1.3×10^{10} m^3/yr in the future during the second project stage. The MSWTP aims to provide more water to promote social and economic growth in North China, which has been restricted by the water supply crisis and ecological degradation [*Liu et al*., 2008].

The Haihe River basin, which receives most of the water input from the MSWTP, is one of the most important agricultural areas in North China (Figure 1a), and it supports the rapidly developing population and industry. This basin includes Beijing, Tianjin, most of Hebei Province, and parts of other provinces, where it accounts for about 74% of the water volume transferred along the conveyance line. Mountains and plateaus are located in the north and west of the basin, and most of the inhabitants live on the eastern and southern plains (Figure 1 b). Due to the high water demand throughout the basin, the groundwater in the plains is exploited rapidly as the major source of water supply [*Xia et al*., 2007]. In Hebei Province, which accounts for most of the area of the plain in the basin, the groundwater supply volume was 16.1×10^9 m^3 in 2005 and the surface water supply was only 3.7×10^9 m^3 [*Ren*, 2007]. The water input from the MSWTP is expected to replace parts of the groundwater exploitation along the conveyance line and to recover the local ecological environment, which has been severely disrupted [*Liu and Zheng*, 2002; *Zhong et al*., 2010].

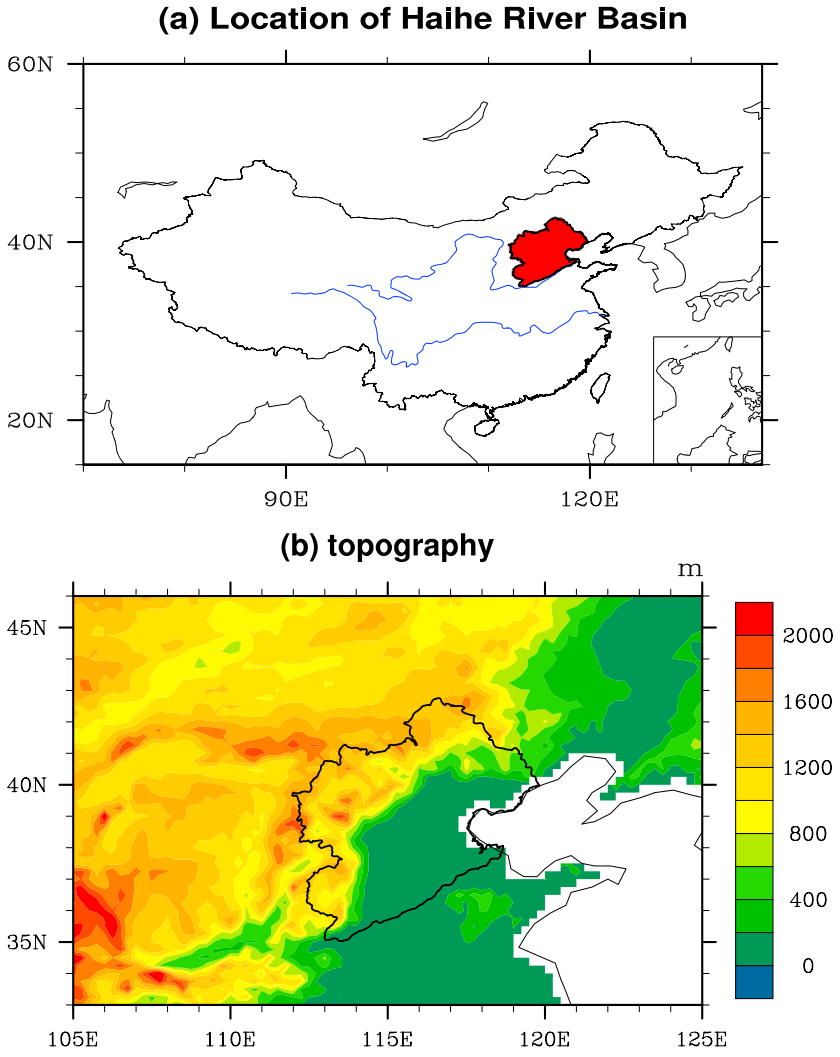

Figure 1. (a) Location of the Haihe River basin in China. The region shaded in red color is the basin. (b) Topography of the Haihe River basin.

The MSWTP started to operate at the end of 2014, but its climatic effects in the Haihe River basin are still not conclusive. Numerous studies have investigated the potential hydrological effects of interbasin water transfer projects such as the MSWTP on their intake areas [*Zhao*, 2002; *Gurung and Bharati*, 2012; *Maknoon et al*., 2012; *Gohari et al*., 2013; *Wang et al*., 2013; *Jia et al*., 2015]. For example, *Pei et al*. [2004] employed a correlation analysis method based on the water balance to analyze the effects of the South-to-North Water Transfer Project, which showed that the water transferred into the basin would increase socioeconomic water usage, but the ecological environment in the estuary area would not be improved. *Yang et al*. [2012] used a groundwater flow model called MODFLOW [*McDonald and Harbaugh*, 1988] to determine the effects of the MSWTP on the groundwater table in the Beijing plain, which showed that the area with depressed groundwater would be reduced and the simulated groundwater table of the depressed area would rise to different extents after receiving the water transferred by the MSWTP. *Ye et al*. [2014] used a large-scale distributed time-variant gain hydrological model to demonstrate that the MSWTP would reduce the rate of decline in the groundwater table over the Haihe River basin and that the area with groundwater overexploitation would decline by 20%.

Most of these previous studies based on hydrological modeling or water balance analysis focused on the responses of the local water resources, groundwater table, or river discharge. In terms of the impacts on regional climate, most studies using climate models have focused on the effects of irrigation [*Boucher*

et al., 2004; *Lobell et al*., 2008; *Sacks et al*., 2009; *Kueppers and Snyder*, 2012]. The climatic effects of the interbasin water transfer projects over the intake area have been investigated in several studies using climate models, but the treatment of the transferred water merits further discussion [*Li and Wang*, 2009; *Okada et al*., 2015]. For example, *Wang et al*. [2007] used the climate model RegCM3 to simulate the regional climate changes over north China after the completion of the MSWTP, where they treated the construction of the MSWTP as large-scale irrigation and the soil moisture was set as saturated during the irrigation period. The results showed that irrigation caused wetting and cooling effects, where the precipitation increased by about 30 mm/yr and the 2 m air temperature decreased by 1–3 K in the summer over North China. *Chen and Xie* [2010] implemented a water transfer mechanism in the climate model RegCM3 to investigate the effects of the MSWTP, where they treated the water transferred as the precipitation reaching the land surface, and they demonstrated that the MSWTP caused increased precipitation of 12.9–21.6 mm/yr and a decrease in the mean 2 m air temperature of 0.12–0.2 K over the North China Plain.

In these studies, the entire water input from the MSWTP was assumed to increase irrigation, and the climatic effects of the MSWTP were regarded as the differences between the assumed irrigation simulations and nonirrigation simulations. In fact, the irrigation process had existed over North China before the construction of the MSWTP and the assumptions were not sufficiently reasonable to increase the irrigation water by about 9.5×10^9 m^3/yr (the approximate volume of water being transferred) after the construction of the MSWTP. Indeed, according to the Committee Office of South-to-North Project Construction (http://www.nsbd.gov.cn/), it was claimed that the water input provided by the MSWTP was definitely used not for irrigation, but instead, it was employed for domestic and industrial consumption. At present, the actual irrigation consumption data for China during 2015 have not been released so no direct data are available to indicate the changes in water consumption after the construction of the MSWTP. As an alternative, the precipitation data derived in this study may indirectly reflect the changes in irrigation. Precipitation has been shown to have a highly negative correlation with irrigation consumption and it has been used as primary climate factor to estimate irrigation demand [*Sadeghi et al*., 2010; *Dominguez-Faus et al*., 2013; *Rehana and Mujumdar*, 2013]. According to the Hebei Province Meteorological Bureau, the annual precipitation over Hebei Province was 505.8 mm/yr in 2015 and it approached the climatological value of 503.7 mm/yr. Thus, due to the sufficient moisture conditions, the irrigation demand would not have increased significantly throughout the intake area. There is a rather low probability that the construction of the MSWTP will cause an explosive increase in irrigation as supposed by *Wang et al*. [2007] and *Chen and Xie* [2010]. Therefore, the primary impact of the MSWTP is not a result of increased irrigation, but instead, it essentially reduces the exploitation of local water resources.

In this study, we coupled the regional climate model RegCM4 with a groundwater exploitation scheme to simulate the climate changes caused by the construction of the MSWTP. We considered anthropogenic water exploitation and consumption, and the water transferred by the MSWTP was also added to the balance of the water supply and consumption over the intake area. The Haihe River basin in North China was selected as the study domain.

2. Methodology

2.1. Model Description

The regional climate model RegCM4 was developed by the International Center for Theoretical Physics in Italy [*Giorgi and Anyah*, 2012; *Giorgi et al*., 2012]. It has been employed in many regions throughout the world and it performs well at simulating the regional climate [*Ozturk et al*., 2012; *Sylla et al*., 2012]. RegCM4 employs three convective precipitation schemes (Kuo, Grell, and Emanuel) and one large-scale precipitation scheme (SUBEX) to simulate precipitation [*Giorgi et al*., 1993]. The land surface physical schemes available in RegCM4 include BATS1e and the Community Land Model version 3.5 (CLM3.5) [*Oleson et al*., 2008].

CLM3.5 is a land surface model developed by the National Center of Atmospheric Research as part of the Community Climate System Model. It contains five possible snow layers, 10 soil layers, and an unconfined aquifer. The groundwater component is based on the simple groundwater model developed by *Niu et al*. [2007], and the unconfined groundwater table can be within or below the soil layers, depending on the changes in water storage.

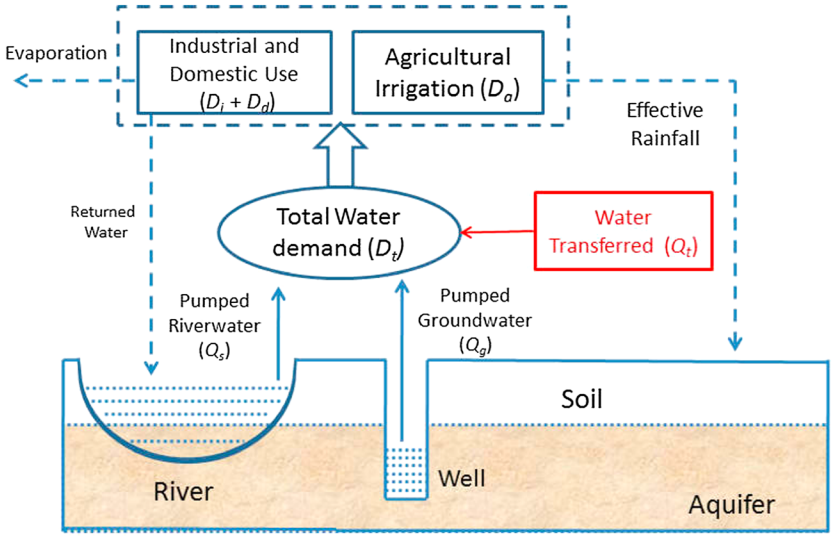

Figure 2. Framework of the water resource exploitation and consumption scheme. The total water demand (D_t, units: kg/m^2/s) is supplied by the water transferred (Q_t, units: kg/m^2/s) as well as water resources pumped from rivers (Q_s, units: kg/m^2/s) and wells (Q_g, units: kg/m^2/s). The total water demand is divided into agricultural irrigation (D_a, units: kg/m^2/s), industrial (D_i, units: kg/m^2/s), and domestic uses (D_d, units: kg/m^2/s). The industrial and domestic uses are considered to partly increase evaporation and partly returned to river channels. The agricultural irrigation is treated as effective rainfall reaching the top soil.

2.2. Water Transfer Scheme Description

In our previous work, a scheme was established to simulate the anthropogenic water exploitation and consumption process [*Zou et al.*, 2014] based on the CLM3.5. In this study, we employed this scheme to investigate the climatic effects of MSWTP. A schematic diagram of this scheme is shown in Figure 2. In the scheme, the groundwater and surface water resources are withdrawn to meet the water demand, and the consumption is divided into three types: industrial, domestic, and irrigation uses. This scheme is based on the balance of the water demand and supply, which can be described by the following equation:

$$Q_s + Q_g = D_a + D_i + D_d = D_t, \tag{1}$$

where Q_s is the volume of exploited surface water resources per unit time and area (kg/m^2/s), Q_g is the volume of exploited groundwater resources (kg/m^2/s), D_a is the water demand due to agricultural irrigation consumption (kg/m^2/s), D_i is the water demand due to industrial consumption (kg/m^2/s), D_d is the water demand due to domestic consumption (kg/m^2/s), and D_t is the total water demand (kg/m^2/s). The three water demand components, i.e., D_a, D_i, and D_d, are preset based on the corresponding estimated data sets.

After receiving the water transferred by the MSWTP, the relationship between the water demand and supply over the intake area can be described by:

$$Q_s + Q_g + Q_t = D_a + D_i + D_d = D_t, \tag{2}$$

where Q_t is the supply of water transferred by the MSWTP (kg/m^2/s) which is preset based on the water transfer data. The exploitation priority for the three supply sectors is set as $Q_t > Q_s > Q_g$. The water transferred by the MSWTP is assumed to be stored in local reservoirs or lakes, and in each time step, a certain volume of stored water Q_t is withdrawn as part of the water supply to satisfy the demand. The exploited surface water Q_s is supplied by the local runoff and streamflow in each grid, which is calculated by

$$Q_s = \min\left[R_t + R_{\mathrm{str}}, \max(D_t - Q_t, 0)\right], \tag{3}$$

where R_t is the total runoff (kg/m^2/s) and R_{str} is the streamflow (kg/m^2/s) flowing into the grid per unit time and area. The exploited groundwater Q_g withdrawn from the aquifers has the lowest priority in the three supply sectors, and it is calculated by

$$Q_g = D_t - Q_s - Q_t. \tag{4}$$

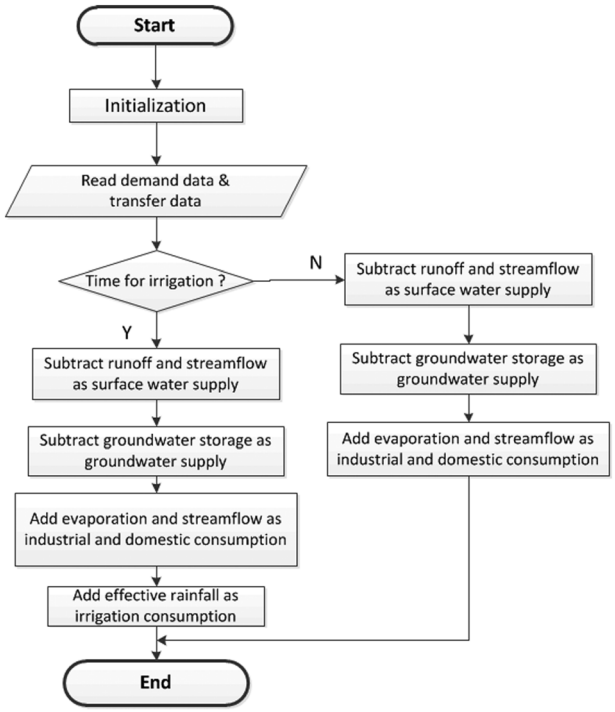

Figure 3. Flowchart illustrating the water transfer scheme.

Although this rarely occurs in the grid cells, Q_g allows itself to be negative if the preset Q_t is larger than D_t, and the negative Q_g will be added into the groundwater storage.

In the consumption process, the industrial and domestic water demands (D_i and D_d) are considered to increase evaporation and local streamflow, and irrigation D_a is considered to increase the effective rainfall reaching the top soil. For the schedule of the consumption process, the industrial and domestic water exhibits no seasonal differences, and the irrigation dates are preset based on the phenology of winter wheat and summer maize, i.e., from 10 March to 18 June and from 22 June to 28 August. In addition, the water transferred Q_t is also set without seasonal differences like D_i and D_d, because the MSWTP only supplies the industrial and domestic consumption requirement, which rarely change significantly among seasons.

This transfer scheme shares the same time step with the land surface module, and the scheme is invoked in the hydrological module in CLM3.5 as a subroutine. A flowchart illustrating the scheme is shown in Figure 3.

2.3. Water Demand and Transfer Data

The actual officially released water consumption data only contain one annual value, and there are no spatial details throughout the basin. Thus, in the present study, we still employed the data estimated over the basin in 2000 as the grid water demand [*Zou et al.*, 2014], and the total demand in 2000 for each grid, $D_{t,2000}$, was calculated as

$$D_{t,2000} = D_{d,2000} + D_{i,2000} + D_{a,2000} = \rho\lambda^{-1}S^{-1}\left(\gamma_1 A_{\text{pop}} + \beta\gamma_2 A_{\text{GDP}} + \gamma_3 A_{\text{agr}}\right), \quad (5)$$

where ρ is the water density, 1.0×10^3 kg/m^3; λ is the number of seconds in a year, 31,536,000 s/yr; S is the grid area (m^2); γ_1 is the domestic water consumption per capita, 40.64 m^3/capita/yr; γ_2 is the industrial water consumption per yuan, 40.65×10^{-4} m^3/yuan/yr; β is an empirical conversion ratio between gross domestic product (GDP) and industrial output, i.e., 1.42; γ_3 is the irrigation water consumption, 0.414 m^3/ha/yr; A_{pop} is the population per grid (capita); A_{GDP} is the GDP per grid (yuan); and A_{agr} is the cropland area per grid (ha). The parameters, including γ_1, γ_2, and γ_3, were derived from *Water Resource Assessment in Haihe River Basin* [*Ren*, 2007]. The socioeconomic data sets, A_{pop}, A_{GDP}, and A_{agr}, were collected from the Data Center for Resources and Environment of Sciences, Chinese Academy of Sciences (http://www.resdc.cn/english/default.asp) with a spatial resolution of 1×1 km, and they were then averaged onto grids of 30×30 km to match the resolution of RegCM4.

The estimated demand $D_{t,2000}$ was used as the demand proxy in the simulations, but its total value was higher than the actual water consumption, probably because the constant rate of water consumption, the empirical ratio, and the difference in data sources introduced uncertainties. In particular, the irrigation consumption was difficult to determine in the rural regions and there were great uncertainties in the data obtained from different agencies.

In order to obtain the spatial distributions of the water demands from 2001 to 2010, $D_{t,2000}$ was then employed as a reference for scaling up or down with the ratios between the actual consumption value in 2000 and the consumption values from 2001 to 2010. The actual consumption values over the Haihe River

Table 1. Annual Estimated Water Demands and Actual Water Consumption in the Haihe River Basin

Year	Actual Consumption (10^8 m^3/yr)	Estimated Demand (10^8 m^3/yr)
2000	398.4	488.6
2001	392.0	480.8
2002	399.8	490.3
2003	377.0	462.4
2004	368.0	451.3
2005	379.8	465.8
2006	392.7	481.6
2007	384.5	471.5
2008	373.4	457.9
2009	370.0	453.8
2010	369.9	453.7

Basin from 2000 to 2010 were collected from *Water Resource Bulletin of Haihe River Basin* released by the Haihe River Water Conservancy Commission (http://www.hwcc.gov.cn/). Table 1 lists the values for the actual water consumption and the total estimated demands summed over the grids in the basin, which shows that there were no obvious increases or decreases in the water consumption series over 10 years.

For the water transfer data, the water loss along the conveyance line was ignored in this study and the water allocated to each city during the simulation was regarded as the gross water volume. In order to obtain the spatial allocation of the water transferred, Q_t, the gross transfer volume of the MSWTP allocated to each province was derived from the official website (http://www.bjnsbd.gov.cn/tabid/158/), but the further water allocated to cities of these provinces was determined by each province administration. Therefore, the net water volume allocated to each city, which was the actual water received, was collected from the official declaration of the local water conservancy of each city at the end of 2014. Next, the water loss, which was the difference between the gross water transferred and the net water received, was allocated to each city based on the ratio between the net volume for the city and the total net volume. For the second-stage construction with a planned transfer volume of 1.3×10^{10} m^3/yr in the future, no explicit allocation plans have been made for each city, so the current water allocation for each city was used as reference for scaling up based on the ratio between the transfer volume of the first and second construction stages.

Table 2 lists the water volumes allocated to each city in the Haihe River basin. Due to data limitations, the water allocation exhibited no further spatial differences within each city. The resolution of the allocation data was treated as 30×30 km and the spatial distribution of the annual water transferred in the unit area over the basin is shown in Figure 4. More water was allocated to the major cities with high water demands in the basin, such as Beijing (116.5°E, 40°N), Tianjin (117°E, 39°N), and Shijiazhuang (114.5°E, 38°N).

2.4. Experimental Design

In this study, we used the RegCM4 model with the CLM3.5 module to perform a group of simulation tests. The settings used in these tests are shown in Table 3. We aimed to determine the climatic effects of the MSWTP over the intake area, where the groundwater resources have been overexploited for decades. Therefore, two 30 year simulation tests were conducted before the main simulations. One test (H1) simulated the groundwater exploitation process using linearly increasing water demands from 1971 to 2000, which were

Table 2. Water Allocation From the MSWTP to Each City in the Haihe River Basin (Unit: 10^8 m^3/yr)

Province	City	Water Transferred (First Stage)	Water Transferred (Second Stage)
Henan	Jiaozuo	3.39	4.64
	Xinxiang	4.93	6.75
	Hebi	2.07	2.83
	Puyang	1.50	2.05
	Anyang	4.21	5.76
Hebei	Baoding	6.94	9.50
	Handan	4.44	6.08
	Xingtai	4.17	5.70
	Hengshui	3.91	5.35
	Shijiazhuang	11.93	16.32
	Langfang	3.31	4.53
Beijing	Beijing	12.40	16.97
Tianjin	Tianjin	10.20	13.96
Total		73.4	100.44

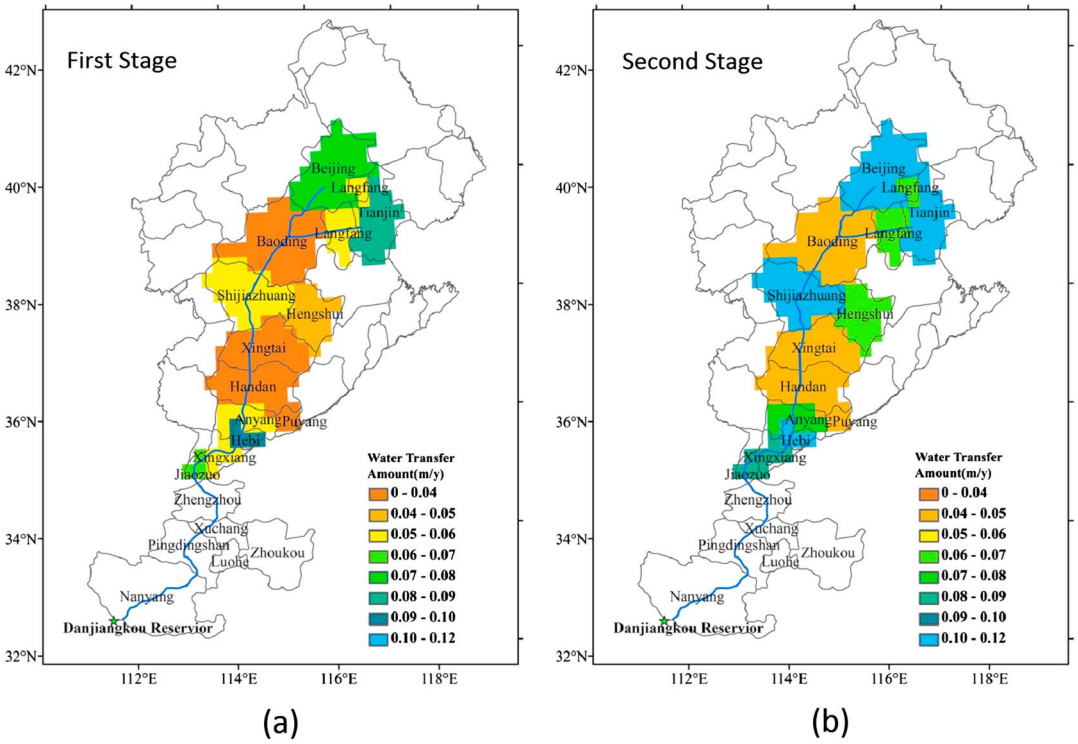

Figure 4. Spatial distributions of the water allocation for the MSWTP in (a) the current first stage of construction and (b) the planned second stage of construction in the Haihe River basin. The blue line indicates the conveyance line of the MSWTP.

linearly fitted based on the historic water consumption values and further details were described in a previous study [*Zou et al*., 2014]. The other test (H0) was conducted as a control without any exploitation. The final status of H1 after exploitation for 30 years was selected as the initial condition for the subsequent main tests instead of the default value in order to simulate the climate after long-term exploitation.

The main simulations comprised four tests from 2001 to 2010. Based on the final status of H1, two transfer tests were conducted to simulate the climate affected by the groundwater exploitation process with the MSWTP. One test (T1) considered the water transfer process with the volume in the current first-stage project and the other test (T2) used the water volume in the planned second-stage project as a sensitivity test to investigate the climatic sensitivity to the transfer volumes. Another exploitation test (T3), which had the same initial conditions as T1 and T2, was designed to continue the exploitation process from 2001 to 2010 without water transfer. In addition, the control test (T0) also continued without any exploitation process based on the final condition of H0.

The spatial resolution of the RegCM4 model was 30 × 30 km and its central location was at 116°E, 38°N. The ERA-40 reanalysis data from 1971 to 2000 were used as lateral boundary forcing in the H1 and H0 tests, and the ERA-Interim reanalysis data from 2001 to 2010 were used as the forcing data in the main tests, i.e., T1, T2, T3, and T0. We selected the CLM option and Grell scheme as the model's land surface scheme and convective precipitation scheme, respectively. The time steps were 30 min for the land surface module and 100 s for the atmospheric module.

Table 3. Descriptions of the Constructed Simulation Tests

	Simulation Period	Initial Condition	Human Activity	Transfer Volume
H1	1971–2000	Final status of a spin-up	Exploitation	None
H0	Same as H1	Same as H1	None	None
T1	2001–2010	Final status of H1	Exploitation + transfer	First stage
T2	Same as T1	Same as T1	Same as T1	Second stage
T3	Same as T1	Same as T1	Exploitation	None
T0	Same as T1	Final status of H0	None	None

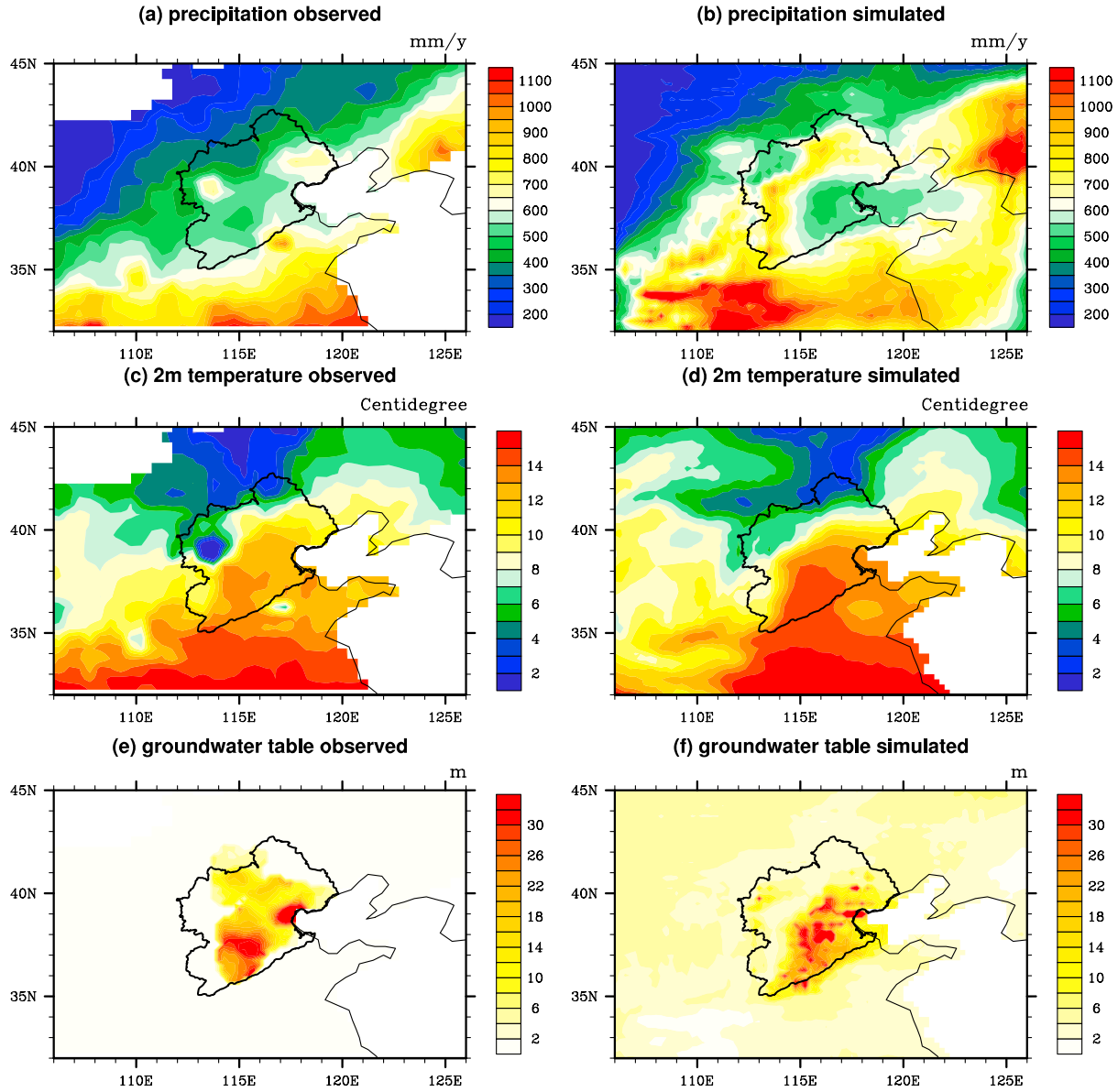

Figure 5. Spatial distributions of (a) mean observed precipitation; (b) precipitation simulated by the H1 test; (c) observed 2 m air temperature; (d) 2 m air temperature simulated by the H1 test; (e) groundwater table depth observed in December 2000; and (f) groundwater table depth simulated by the H1 test in December 2000.

3. Results

3.1. Model Validation

The results of the H1 test from 1971 to 2000 were used to validate the model's simulation capacity. The observed precipitation and temperature data used for comparison were collected from the 740 meteorology stations in China and linearly interpolated with weights based on the inverse distance squared [*Xie et al.*, 2007]. The 30 year mean precipitation, the 2 m air temperature in the H1 test, and the observations are shown in Figures 5a–5d. The simulated precipitation and temperature obtained by the H1 test had similar decreasing slopes compared with the observations from northwest to southeast over the study domain, but a higher temperature of about 1°C was detected over the basin in the H1 test. The simulated precipitation was about 60 mm/yr more than the average observations over the basin, except for the eastern plains, where slightly less precipitation was simulated. Instead of the mean values, Figures 5e and 5f show the distributions of the unconfined groundwater depth in December 2000. The data in Figure 5e were collected from 173

Table 4. Statistical Indices for Precipitation and the 2 m Temperature for the H1 Test

	Correlation Coefficient[a]	Root-Mean-Square Error	Standard Deviation	
			Observation	Simulation
Precipitation	0.75	1.42 mm/d	1.83 mm/d	2.07 mm/d
Temperature	0.87	5.32°C	10.83°C	10.17°C

[a]Correlation coefficient: $CC = \frac{\sum_{i=1}^{n}(x_{mi}-\overline{x_m})(x_{oi}-\overline{x_o})}{\sqrt{\sum_{i=1}^{n}(x_{mi}-\overline{x_m})^2 \cdot \sum_{i=1}^{n}(x_{oi}-\overline{x_o})^2}}$, where x_{mi} and x_{oi} are the simulated and observed mean monthly precipitation or temperature in month i, respectively, and n is the number of months; root-mean-square error: $RMSE = \sqrt{\frac{1}{n}\sum_{i=1}^{n}(x_{mi}-x_{oi})^2}$; standard deviation: $STD = \sqrt{\frac{1}{n}\sum_{i=1}^{n}(x_i-\overline{x})^2}$.

observation wells provided by the Ministry of Water Resource and Institute for Geo-Environmental Monitoring in China. The simulated groundwater depth was basically equivalent to the observations and the depth in the area with high demand even exceeded 30 m. However, the area where the simulated groundwater table dropped most did not agree well with the observations, probably because the lateral flow was not considered in the CLM model and the groundwater flow could not be transferred among the grid cells. The location mismatch between the water supply and consumption also contributed to the spatial bias in Figures 5e and 5f because the water source sites for cities are usually located in areas distant from cities.

In addition to the spatial distribution, the statistical indices for precipitation and temperature in the Haihe River basin are listed in Table 4, including the temporal correlation coefficient, root-mean-square error, and standard deviation. These statistics indicate that the simulated series corresponded to the observations, and thus, the RegCM4 model was able to simulate the temporal variability in the local climate suitably well.

3.2. Spatial Distributions of the Climatic Responses to Water Transfer

As mentioned in section 1, the construction of the MSWTP would not significantly change the total water demand or the water consumption process in the basin, but instead, it would reduce the exploitation of local water resources. Thus, the primary climatic effects of the MSWTP were attributable to the slower rate of exploitation for local water resources. Therefore, we used the results from T3–T0 to represent the climatic changes due to local groundwater exploitation and consumption, and the results from T1–T3 and T2–T3 to indicate further changes due to the construction of the MSWTP and the sensitivity of the climatic response to different transfer volumes. It should be noted that the results from T3–T0 were only used for additional discussion because they were not the focus of this study and the changes were quite similar to those described from 1971 to 2000 in our previous study, which provided a more detailed demonstration.

Figures 6 and 7 show the spatial distributions of the 10 year mean changes due to groundwater exploitation without transfer (T3–T0), as well as the changes due to water transfer in the first-stage (T1–T3) and second-stage (T2–T3) constructions. The spatial distributions of the groundwater depth differences are shown in Figures 6a–6c. As shown in Figure 6a, exploitation for 10 years led to an average decline in the groundwater table of about 3.6 m in the basin during the simulation period. On the eastern plain, which contains most of the population and industrial facilities in the basin, the groundwater table dropped the most, where the areas shaded with stripes exceeded the confidence level of 95%. Compared with T3, the groundwater table still dropped in T1 and T2, but the construction of the MSWTP reduced the declines in the groundwater table. Along the conveyance line, the groundwater table increases corresponded to the distribution of transferred water. For the first-stage construction (Figure 6b), the increases even exceeded 3 m near Beijing (116.3°E, 40°N) and Tianjin (117°E, 39°N), where more water was allocated. The changes in Figure 6c (second-stage construction) are similar to those in Figure 6b, except the increase is higher because more water was transferred.

Throughout the basin, massive amounts of groundwater resources are withdrawn for irrigation and other purposes, thereby leading to higher soil moisture with a rapidly falling groundwater table. Figures 6d–6f show the 10 year mean differences in the soil moisture. Figure 6d demonstrates that the mean soil moisture increased significantly by an average of 0.005 m^3/m^3 throughout the basin. In the area to the northeast of the basin, the soil moisture also increased due to greater precipitation (Figure 7g) as more water vapor was transferred from the basin.

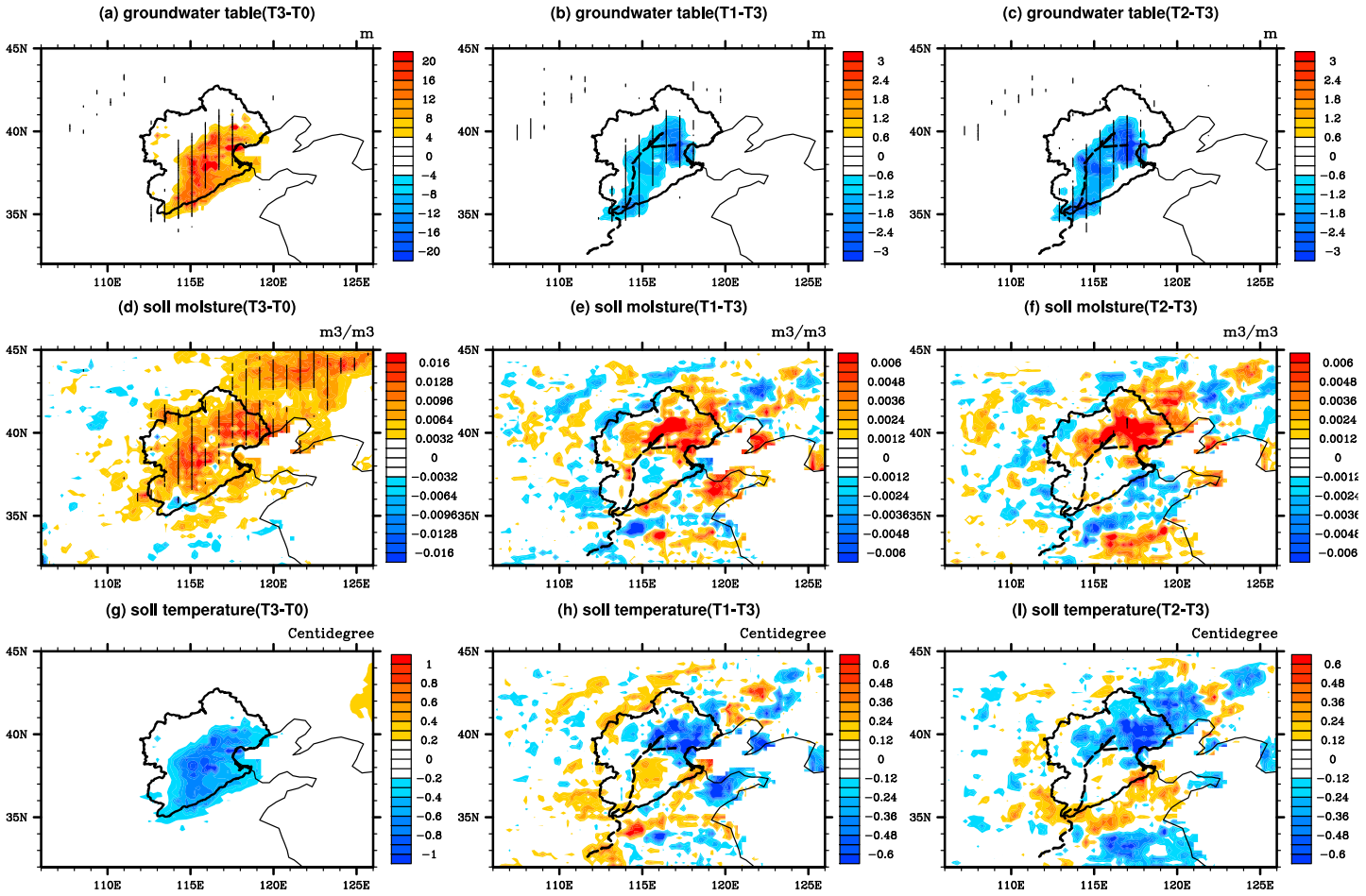

Figure 6. Spatial distributions of (a) mean groundwater table depth (T3–T0); (b) groundwater table depth (T1–T3); (c) groundwater table depth (T2–T3); (d) soil moisture (T3–T0); (e) soil moisture (T1–T3); (f) soil moisture (T2–T3); (g) soil temperature (T3–T0); (h) soil temperature (T1–T3); and (i) soil temperature (T2–T3). The dashed line indicates the conveyance line of the MSWTP and the area shaded by stripes indicates that the changes there are at or exceed the 95% confidence level.

In CLM3.5, the changes in soil moisture are determined by both the changes in upper precipitation and lower groundwater discharge. When the groundwater table falls far deeper than the soil depth, the groundwater recharge q_{recharge} from the soil to the aquifer will approach the maximum infiltration capacity as the groundwater depth approaches infinity. Thus, the rising groundwater table due to water transfer reduces the slowly increased recharge q_{recharge} and the lower soil layers will become wetter if the water flux entering the soil from precipitation remains unchanged. The wetter soil will ultimately provide feedback via changes in the heat fluxes from the soil surface.

Compared with the results from T3–T0, the further changes due to water transfer were not statistically significant. As shown in Figures 6e and 6f, the construction of the MSWTP increased the soil moisture in most of the intake area, except for the southern part of the conveyance line where less water was allocated and slightly drier soil was detected. On average, the soil moisture over the basin increased by 0.0008 m^3/m^3 and 0.001 m^3/m^3 with the first and second stages of construction, respectively.

The increased moisture caused further declines in the soil temperature, which declined by 0.26°C on average in T3 compared with T0 (Figure 6g). The water transfer project slightly enhanced the cooling effects and the mean soil temperature decreases over the basin were 0.04°C and 0.05°C, respectively, in these tests (Figures 6h and 6i).

The mean latent heat flux over the basin (Figure 7a) increased by about 3.2 W/m^2 on average in T3, whereas the sensible heat flux (Figure 7d) decreased by 2.2 W/m^2. With more moisture in the soil, the water transfer process led to further increases in the latent heat and decreases in the sensible heat from the soil to the upper

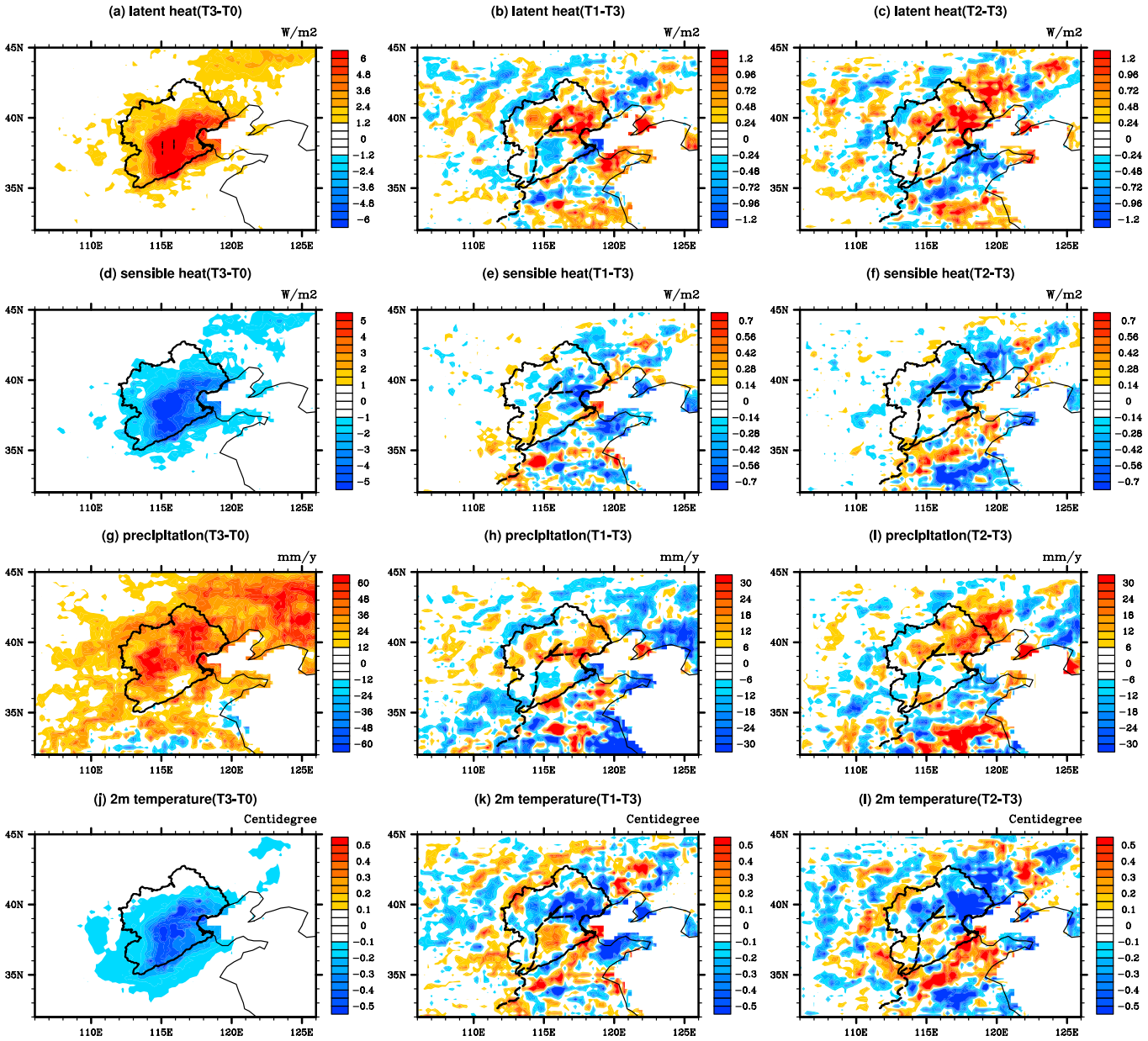

Figure 7. Spatial distributions of (a) mean latent heat flux (T3–T0); (b) latent heat flux (T1–T3); (c) latent heat flux (T2–T3); (d) sensible heat flux (T3–T0); (e) sensible heat flux (T1–T3); (f) sensible heat flux (T2–T3); (g) precipitation (T3–T0); (h) precipitation (T1–T3); (i) precipitation (T2–T3); (j) 2 m air temperature (T3–T0); (k) 2 m air temperature (T1–T3); and (l) 2 m air temperature (T2–T3). The dashed line indicates the conveyance line of MSWTP and the area shaded by strips indicates that the changes there are at or exceed the 95% confidence level.

atmosphere. As shown in Figures 7b and 7c, the mean latent heat flux increases were about 0.08 W/m^2 and 0.12 W/m^2 over the basin due to water transfer, which were far less than the changes caused by the water consumption process in T3. According to Figures 7d and 7e, the average decreases in the magnitudes of the sensible heat flux were less than those of the latent heat, i.e., 0.05 W/m^2 for the first-stage construction and 0.07 W/m^2 for the second stage. In agreement with the changes in soil moisture, the areas where the heat fluxes changed most were also located to the north of the basin at the end of the conveyance line.

The changes in the heat fluxes emitted from the land surface will affect the upper atmosphere, thereby providing further feedback via precipitation and radiation. As shown in Figure 7g, the water consumption process over the basin increased the moisture at the land surface, as well as leading to more local precipitation. On average, the precipitation increased by about 33 mm/yr due to the water consumption processes in

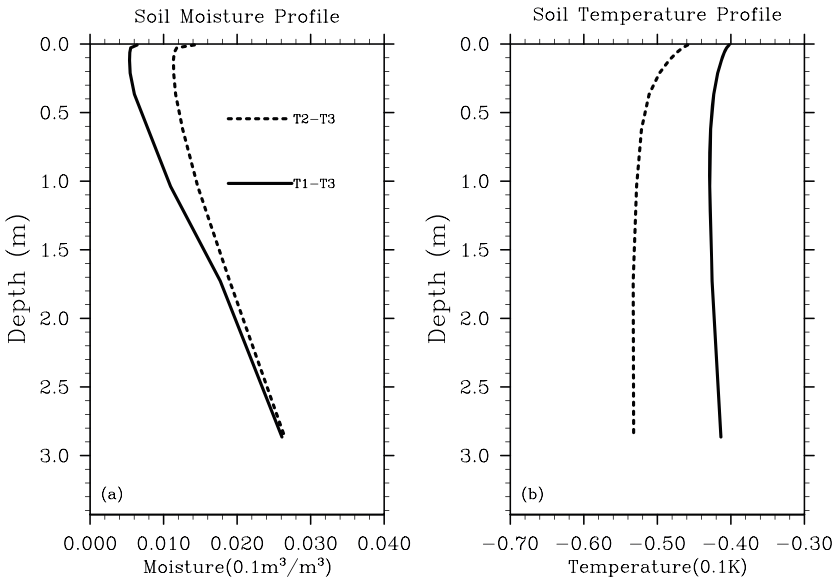

Figure 8. Vertical profiles of the mean differences in (a) soil moisture and (b) soil temperature averaged over the basin.

the basin. More precipitation was also detected in the region to the northeast of the basin, thereby leading to higher soil moisture in this area. However, the construction of the MSWTP did not cause obvious further increases in precipitation throughout the basin due to its weak effects on land-atmosphere interactions. The mean increases in precipitation were only 1.2 mm/yr and 2.0 mm/yr for the whole basin (Figures 7h and 7i). For the second-stage construction shown in Figure 6i, the increase in precipitation even exceeded 20 mm/yr in some northern regions of the basin, but these obvious changes were still limited to a local scale and they did not cover the whole basin similar to the changes shown in Figure 7g. The increases in convective precipitation (not shown) accounted for most of the changes in precipitation, with mean increases by 0.93 mm/yr and 1.55 mm/yr.

The mean changes in the 2 m air temperature shown in Figures 7j–7l are similar to those in the soil temperature, except for their magnitudes. In T3, the mean 2 m temperature decreased by 0.2°C over the basin compared with T0. However, when we compared T3 with both of the transfer tests, as shown in Figures 7k and 7l, further cooling effects were only detected in the northern area of the basin where more water was transferred. When averaged over the basin scale, the construction of the first-stage and second-stage projects only led to decreases of 0.02°C and 0.03°C, respectively.

According to *Chen and Xie* [2010], if the entire water transferred was used to increase irrigation consumption, the changes would comprise increases of 5.6–8.9 W/m^2 for latent heat, decreases of 4.3–7.0 W/m^2 for sensible heat, decreases of 0.12–0.2°C for 2 m air temperature, and increases of 12.9–21.6 mm/yr for precipitation, which correspond to different transfer volumes. However, provided that the water consumption generally remained the same levels as when they conducted their research in previous years, our simulation showed that the climate feedbacks due to this water transfer were nearly less than 10% of the changes presented by *Chen and Xie* [2010], rooted in the different water-consuming ways. In brief, according to our results, the construction of the MSWTP enhanced the cooling and wetting effects at the land surface through human-induced water consumption processes in the basin. However, the climatic effects of the MSWTP itself were weaker than the changes caused by preexisting water consumption through local groundwater and surface water exploitation in the basin, since that majority of the water transferred contributes to reduced local groundwater consumption. The additional cooling and wetting effects due to water transfer were only detected in the northern area of the basin, where more water was transferred.

3.3. Vertical Changes and Temporal Variations in the Climatic Response to Water Transfer

The mean profiles of the spatially averaged soil moisture and temperature throughout the basin are shown in Figures 8a and 8b. The changes due to water exploitation and consumption (T3–T0), which have been

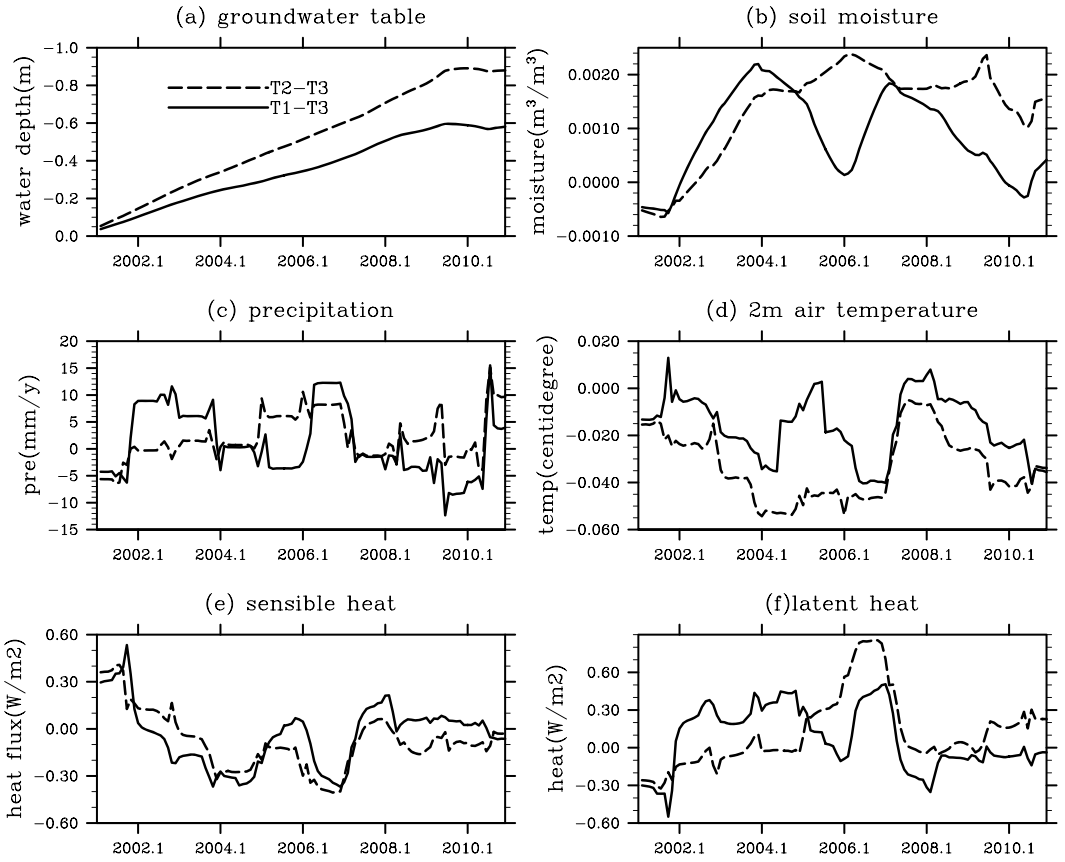

Figure 9. Time series of the differences in (a) groundwater table depth (downward is positive on the vertical axis); (b) soil moisture; (c) precipitation; (d) 2 m air temperature; (e) sensible heat flux; and (f) latent heat flux.

demonstrated previously, are not described in this section. As shown in Figure 8a, the transferred water increased the moisture in each soil layer on average, and the increase in magnitude increased with the depth. The maximum increase appeared in the bottom layers, thereby indicating that the decrease in groundwater recharge from the lower soil layers clearly increased the soil moisture in these layers. Wetter soil due to increased precipitation was also detected in the top soil layer. However, the increased moisture in the top layers was still less than that in the bottom layers. The moisture profile indicated that the construction of the MSWTP led to wetter soil in all layers throughout the basin, where the increased moisture was due mainly to a rising groundwater table and decreased groundwater recharge. The increased precipitation also played a positive role throughout the basin, but its wetting effects were less important. The difference between T1–T3 and T2–T3 declined with depth and it almost approached zero at the bottom layer, thereby indicating that the weaker wetting effects of T1–T3 at the bottom were not as strong as those of T2–T3 in affecting the moisture in the upper layers.

In CLM3.5, the soil layers are thermally isolated from the aquifer and the thermal conductivity coefficient does not change acutely with the soil depth. Thus, the changes in soil temperature depend only on the energy flux into the soil surface, which is different from the soil moisture. As shown in Figure 8b, the further cooling effects on soil due to water transfer did not vary greatly in the lower depths, whereas there was a slight decline in the top layers. The difference between T1–T3 and T2–T3 remained at 0.01°C to 0.015°C and it increases slightly with depth.

Figure 9 shows monthly series of the main climatic variables at the land surface for T1–T3 and T2–T3 throughout the basin. In these series, the 12 month moving average is used to remove seasonal variations. As shown in Figure 9a, the groundwater table rose slowly due to water transfer. At the end of 2010, compared with T3, the groundwater table height increased by about 0.6 m and 0.9 m throughout the basin in the first-stage and second-stage transfer tests, respectively. In the areas where more water was transferred, such as the regions

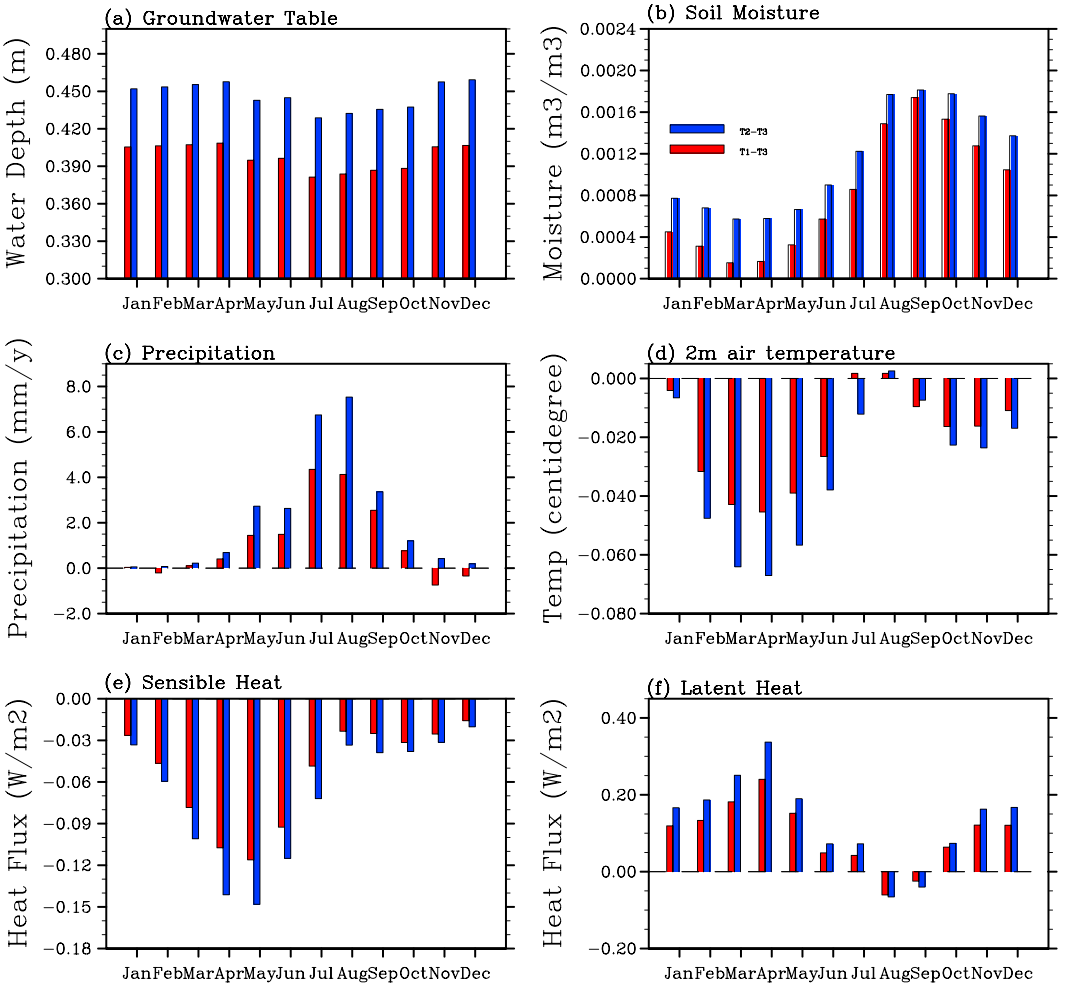

Figure 10. Mean monthly differences in (a) groundwater table depth; (b) soil moisture; (c) precipitation; (d) 2 m air temperature; (e) sensible heat flux; and (f) latent heat flux.

near Beijing and Tianjin, the increase in height was much greater than the average level. However, the groundwater table in the transfer tests still dropped throughout the basin despite the water transfer compared with the control test T0. Thus, the water transfer process only slowed down the drop in the groundwater table because less water was transferred than the total demand.

Due to the weak effects of water transfer on the local climate, the series for the other variables did not exhibit obvious trends like the groundwater table. Figure 9b shows monthly series for the soil moisture differences. This variable links groundwater and the upper atmosphere, so the moisture series for T2–T3 did not exhibit similar temporal variations to T1–T3, which differed from the series for the other variables at the land surface. Instead, the peak values for T2–T3 were delayed for tens of months. For the precipitation and 2 m air temperature shown in Figures 9c and 9d, the series fluctuated around zero and slight enhancements of the fluctuating altitude were detected in the series for T2–T3, which obtained wetter and cooler simulations of the land surface. Figures 9e and 9f show monthly series for the sensible heat and latent heat flux, where the increase in the latent heat flux was slightly higher than the decrease in the sensible heat flux for the T1–T3 and T2–T3 series.

The seasonal variations in T1–T3 and T2–T3 are also shown in Figure 10. As shown in Figure 10a, the groundwater table depth exhibited no obvious seasonal variations because the transfer water was allocated with no differences within 1 year in the transfer tests. The rise in the groundwater table was only slightly greater in the dry season than that in the rainy season. The total effects of the rising groundwater depth on the soil moisture were greater than the effects of increased precipitation (Figure 8g). However, this conclusion did not

apply to all seasons. As shown in Figure 10b, we detected large seasonal variations in soil moisture in contrast to the groundwater depth in Figure 10a. The greatest increase in soil moisture occurred from August to October, which is the main rainy season in the Haihe River basin. A lower increase in the soil moisture was detected in spring when the basin receives less precipitation and the increased moisture was mainly caused by the relatively high groundwater depth. In most months, the increased moisture in T2–T3 was higher than that in T1–T3, which corresponded to the greater volume of water transferred.

The largest differences in precipitation (Figure 10c) occurred in the rainy seasons from June to September because the precipitation was less in other seasons compared with summer and early autumn. For the relative differences in precipitation (not shown), the largest ones still occurred in summer and early autumn, despite that their seasonal differences were less than the absolute differences in Figure 10c. The seasonal variations in the 2 m air temperature and heat fluxes shown in Figures 10d–10f corresponds well to each other, with the largest difference detected in the spring when the air was drier and the heat fluxes were more sensitive to soil moisture. A slight increase in soil moisture could have led to a larger latent heat flux change than those in the summer or early autumn when the heat fluxes were less sensitive to the changes of moisture at the land surface due to more precipitation and air humidity. The annual distributions indicated that the construction of the MSWTP led to further increases in precipitation and soil moisture during the summer or early autumn. However, the enhancement of wetting effects due to the MSWTP was more significant for the changes in the heat fluxes during the spring than the other seasons.

4. Conclusion and Discussion

In this study, we developed and implemented a water transfer scheme using the regional climate model RegCM4. We designed a group of simulation tests to investigate the climatic effects of the MSWTP on the Haihe River Basin, i.e., one control test (T0) without water exploitation, one exploitation test (T3), and two transfer tests that considered both water exploitation and transfer based on the water volumes in the current first-stage (T1) and planned second-stage transfer projects (T2). The tests were conducted from 2001 to 2010 based on the final status of a 30 year groundwater exploitation simulation from 1971 to 2000. By comparing the changes in T3 –T0, T1 –T3, and T2–T3, we demonstrated the climatic effects of groundwater exploitation and further changes due to water transfer.

The main conclusions of this study are as follows. (1) Huge volumes of groundwater resources are exploited for human consumption throughout the basin, which has led to rapid declines in the groundwater table depth, with significant wetting and cooling effects at the land surface. (2) The construction of the MSWTP will reduce the drop in the groundwater table due to exploitation if the same level of water consumption is maintained in the basin. In particular, we found that the groundwater table in the basin rose by about 0.6 m and 0.9 m at the end of the simulation periods for the first stage (T1) and second stage (T2) of construction, respectively, compared with the exploitation test T3 without water transfer. The relative increases in the groundwater table caused by the MSWTP-induced increases in the soil moisture in the lower layers as well as enhancing the wetting and cooling effects at the land surface. Slight increases in the latent heat flux and precipitation, as well as decreases in the 2 m air temperature, soil moisture, and sensible heat flux were detected in most areas along the conveyance line, especially in the areas near Beijing and Tianjin, which received more water. (3) The further wetting and cooling effects of water transfer were rather weak and they exhibited no obvious interannual trends. Within a year, the effects of water transfer depended mainly on the seasonal variations in the local climate. The greatest changes occurred during the summer for precipitation and soil moisture, and in spring for the energy-related variables (heat fluxes and 2 m air temperature). In addition, there were no obvious differences in the spatial distributions and temporal variations for the effects of the first and second stages of construction. In general, the effects of water transfer were also positively related to the water volume transferred.

This study demonstrates the possible climatic effects of the construction of the MSWTP on the Haihe River basin. However, the data estimates, transfer scheme design, and structural defects in CLM3.5 introduced uncertainties into the simulation results. For example, the water transfer data used in this study only included the total annual volumes for each city. Thus, more detailed data are needed for the allocation scheme to distribute the water along the conveyance line more accurately. The estimated total water demand data also exhibited some bias in terms of the actual consumption value. Further improvements should be addressed

to estimate the irrigation demands more accurately and to obtain more detailed distributions of annual water demands during the simulation period. The scheme used in this study highly simplified the water exploitation and consumption processes, and efforts should be made to obtain more reasonable approximations of the water consumption sectors, too.

The defects in the hydrological components of CLM3.5 also introduced uncertainties. The lateral flow process for groundwater is not included in RegCM4/CLM3.5. Thus, the groundwater statuses of the grid cells are isolated from each other and the drop in the groundwater depth is only determined by the exploitation rate in each grid. Due to the lack of groundwater lateral flow, the simulated spatial distributions of the groundwater depth were very different from the observations. In addition, the water volumes of lakes or reservoirs could not be specified in the model. The absence of lakes led to low exploitation of the surface water resources during the simulation, and the water transfer process could only be described indirectly in the water exploitation scheme.

To improve the current findings, further efforts should be made to obtain more accurate data estimates, reasonable descriptions of the water consumption process, as well as introducing groundwater lateral flow and the lake water volumes into the CLM model in the future.

Acknowledgments
This study was partially supported by the National Key Basic Research Program of China (973 Program) under grant 2015CB452701, the Natural Science Foundation of China (grant 41571019), and the Youth Foundation of Shandong Academy of Sciences, China (grant 2014QN035). The related results in this manuscript were stored on local disk and could be requested through zoujing@mail.iap.ac.cn.

References

Boucher, O., G. Myhre, and A. Myhre (2004), Direct human influence of irrigation on atmospheric water vapor and climate, *Clim. Dyn.*, *22*(6), 597–603.

Chen, F., and Z. Xie (2010), Effects of interbasin water transfer on regional climate: A case study of the Middle Route of the South-to-North Water Transfer Project in China, *J. Geophys. Res.*, *115*, D11112, doi:10.1029/2009JD012611.

Dominguez-Faus, R., C. Folberth, J. Liu, A. M. Jaffe, and P. J. Alvarez (2013), Climate change would increase the water intensity of irrigated corn ethanol, *Environ. Sci. Technol.*, *47*, 6030–6037.

Giorgi, F., and R. Anyah (2012), The road towards RegCM4, *Clim. Res.*, *52*, 3–6.

Giorgi, F., M. Marinucci, G. Bates, and G. Canio (1993), Development of a second-generation regional climate model (RegCM2): Part II. Convective processes and assimilation of lateral boundary conditions, *Mon. Weather Rev.*, *121*, 2814–2832.

Giorgi, F., et al. (2012), RegCM4: Model description and preliminary tests over multiple CORDEX demains, *Clim. Res.*, *52*, 7–29.

Gohari, A., S. Eslamian, A. Mirchi, J. Abedi-Koupaei, A. Bavani, and K. Madani (2013), Water transfer as a solution to water shortage: A fix that can Backfire, *J. Hydrol.*, *491*, 23–29.

Gurung, P., and L. Bharati (2012), Downstream impacts of the Melamchi Inter-Basin Water Transfer Plan (MIWTP) under current and future climate change projections, *Hydro Nepal: J. Water Energy Environ. Spec. Issue*, 23–29.

Jia, H., S. Liang, and Y. Zhang (2015), Assessing the impact on groundwater safety of inter-basin water transfer using a coupled modeling approach, *Font. Environ. Sci. Eng.*, *9*(1), 84–95.

Kueppers, L. M., and M. A. Snyder (2012), Influence of irrigated agricultural on diurnal surface energy and water fluxes, surface climate, and atmospheric circulation in California, *Clim. Dyn.*, *38*, 1017–1029.

Li, J., and H. Wang (2009), Regional climate effects of large-scale agricultural irrigation related to South-to-North Water Transfer Project in China [in Chinese], *Adv. Water Sci.*, *20*(3), 343–349.

Liu, C. (1994), South-to-north water transfer in China, *Chin. Environ. Dev.*, *5*(2), 1–15.

Liu, C., and H. Zheng (2002), South-to-north water transfer schemes for China, *Water Resour. Dev.*, *18*(3), 453–471.

Liu, J., C. Zheng, L. Zheng, and Y. Lei (2008), Ground water sustainability: Methodology and application to the North China Plain, *Ground Water*, *46*(6), 897–909.

Lobell, D. B., C. J. Bonfils, L. M. Kueppers, and M. A. Snyder (2008), Irrigation cooling effect on temperature and heat index extremes, *J. Geophys. Res.*, *35*, L09705, doi:10.1029/2008GL034145.

Maknoon, R., M. Kazem, and M. Hasanzadeh (2012), Inter-basin water transfer projects and climate change: The role of allocation protocols in economic efficiency of the project. Case study: Dez to Qomrood Inter-Basin Water Transmission Project (Iran), *J. Water Resour. Protect.*, *4*(9), 750–758.

McDonald, M. G., and A. W. Harbaugh (1988), A modular three dimensional finite difference ground water flow model, U.S. Geol. Surv. Open File 83-875, 6.

Niu, G., Z. Yang, R. Dickinson, L. Gulden, and H. Su (2007), Development of a simple groundwater model for use in climate models and evaluation with gravity recovery and climate experiment data, *J. Geophys. Res.*, *112*, D07103, doi:10.1029/2006JD007522.

Okada, M., T. Iizumi, G. Sakurai, N. Hanasaki, T. Sakai, K. Okamoto, and M. Yokozawa (2015), Modeling irrigation-based climate change adaptation in agriculture: Model development and evaluation in Northeast China, *J. Adv. Model. Earth Syst.*, *7*, 1409–1424, doi:10.1002/2014MS000402.

Oleson, K., et al. (2008), Improvements to the Community Land Model and their impact on the hydrological cycle, *J. Geophys. Res.*, *113*, G01021, doi:10.1029/2007JG000563.

Ozturk, T., H. Altinsoy, M. Turkes, and M. Kurnza (2012), Simulation of temperature and precipitation climatology for the Central Asia CORDEX domain using RegCM4.0, *Clim. Res.*, *52*, 63–76.

Pei, Y., J. Wang, and L. Luo (2004), Analysis of effect of South-to-North Water Transfer Project on aquatic ecosystems of Haihe River basin [in Chinese], *Acta Ecol. Sin.*, *24*(10), 2115–2123.

Rehana, S., and P. P. Mujumdar (2013), Regional impacts of climate change on irrigation water demands, *Hydrol. Process.*, *27*(20), 2918–2933.

Ren, X. (2007), *Water Resource Assessment of Haihe River Basin* [in Chinese], China Water Power Press, Beijing, China.

Sacks, W. J., B. I. Cook, N. Buenning, S. Levis, and J. H. Helkowski (2009), Effects of global irrigation on the near-surface climate, *Clim. Dyn.*, *33*(2), 159–175.

Sadeghi, A., M. G. B. Mohayidin, M. A. B. Hussein, and J. Attari (2010), Estimation of irrigation water demand for Barley in Iran: The panel data evidence, *J. Agric. Sci.*, *2*(2), 31–40.

Shan, F., X. Ling, G. Zhi, and L. Jin (2007), Assessing the impacts of South-to-North Water Transfer Project with decision support systems, *Decis. Support Syst. Emerging Econ.*, *42*(4), 1989–2003.

Sylla, M., F. Giorgi, and F. Stordal (2012), Large-scale origins of rainfall and temperature bias in high-resolution simulations over southern Africa, *Clim. Res.*, *52*, 193–211.

Wang, C., Y. Wang, and P. Wang (2006), Water quality modeling and pollution control for the eastern route of South to North Water Transfer Project in China, *J. Hydrodyn.*, *18*(3), 253–261.

Wang, H., J. Li, Y. Ju, and C. Yang (2007), The regional climate effects of large-scale agricultural irrigation related to south-to-north water transfer engineering in China, *Proc SPIE Remote Sens. Model. Ecosyst. Sunstainability IV*, *6679*, 66791R, doi:10.1117/12.731096.

Wang, L., D. Yan, H. Wang, J. Yin, and Y. Bai (2013), Impact of the Yalong-Yellow River water transfer project on the eco-environment in Yalong River basin, *Sci. China Technol. Sci.*, *56*(4), 831–842.

Xia, J., L. Zhang, C. Liu, and J. Yu (2007), Towards better water security in North China, *Water Resour. Manage.*, *21*(1), 233–247.

Xie, Z., F. Yuan, Q. Duan, J. Zheng, M. Liang, and F. Chen (2007), Regional parameter estimation of the VIC land surface model: Methodology and application to river basins in China, *J. Hydrometeorol.*, *8*(3), 447–468.

Yang, Y., G. Li, Y. Dong, M. Li, J. Yang, D. Zhou, Z. Yang, and F. Zheng (2012), Influence of south to north water transfer on groundwater dynamic change in Beijing plain, *Environ. Earth Sci.*, *65*, 1323–1331.

Ye, A., Q. Duan, W. Chu, J. Xu, and Y. Mao (2014), The impact of the South-North Water Transfer Project (CTP)'s central route on groundwater table in the Hai River basin, North China, *Hydrol. Process.*, *28*, 5755–5768.

Zhao, M. (2002), A theoretical analysis on the effect of water transportation from south to north China on the local climate in the northern part of China, *J. Nanjing Univ.*, *38*(3), 271–280.

Zhong, H., J. Bian, and W. Li (2010), Groundwater protection and remediation measures for the water imported areas of the south-to-north water diversion, *China Water Resour.*, *7*, 33–35.

Zou, J., Z. Xie, Y. Yu, C. Zhan, and Q. Sun (2014), Climatic responses to anthropogenic groundwater exploitation: A case study of the Haihe River basin, Northern China, *Clim. Dyn.*, *42*(7-8), 2125–2145.